ChemComm

Accepted Manuscript

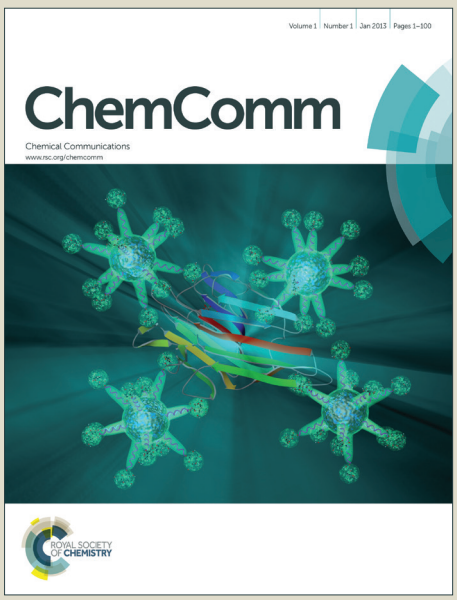

ROYAL SOCIETY OF CHEMISTRY

www.rsc.org/chemcomm

Journal Name

RSCPublishing

COMMUNICATION

Cryo-generated Ferrous-superoxo Porphyrin: EPR, Resonance Raman and DFT studies

Cite this: DOI: 10.1039/x0xx00000x

Takehiro Ohta,[a,b,*] Jin-Gang Liu,[b,c,*] Perumandla Nagaraju,[b] Takashi Ogura[a] and Yoshinori Naruta[b,d,*]

Received 00th April 2015,
Accepted 00th June 2015

DOI: 10.1039/x0xx00000x

www.rsc.org/

Resonance Raman analysis of cryo-generated ferrous-superoxy heme is performed for the first time, and its structure and reaction mechanism are rationalized by DFT calculations. The presence of another electronic tautomer of ferrous-superoxy heme is predicted computationally.

Studies of the structure/reactivity correlations of partially reduced oxygen species (PROS) of iron porphyrin adducts are essential in order to characterize the biological dioxygen activation mechanism. Such studies are expected to provide the necessary insights to design efficient molecular catalysts.[1-7] In the dioxygen reduction reaction (ORR), the first one electron reduction process is the most energy demanding and has a large overpotential.[8] In nature, this step is overcome using ferrous iron porphyrin, wherein free energy gained through binding of dioxygen to the ferrous iron drives single electron reduction of O_2 to yield a ferric-superoxo species.[9-12] Subsequent electron transfer to the ferric-superoxo complex may yield either a ferric-peroxo [Fe^{III}-(O_2^{2-})] or a ferrous-superoxo [Fe^{II}-($O_2^{\bullet-}$)] species. These two species are electronic tautomers which differ with respect to occupation of electrons among the Fe d and O_2 valence orbitals.[13] When electron transfer is coupled with protonation, a ferric hydroperoxo species is formed.[14-18] This species undergoes O-O bond cleavage to yield a highly oxidized iron porphyrin. While several spectroscopic studies have focused on highly oxidized intermediates,[19] there have been relatively few vibrational spectroscopic studies of peroxy level intermediates despite their key roles in the generalized ORR mechanism.[7,14,20,21] Since the ferrous superoxy adduct of heme has been characterized solely on the basis of EPR spectroscopy,[22,23] further concrete experimental evidence of its structure is desired. Herein, we present the first resonance Raman (rR) characterization of the ferrous-superoxy heme intermediate, which is prepared by cryo-reduction by γ-ray irradiation of a ferric-superoxo precursor dissolved in a frozen aprotic solvent. New insights into the structure and reactivity of the ferrous-superoxo heme complex are gained through DFT calculations. In addition, another electronic tautomer of the ferrous-superoxo heme is described.

The single electron reduction of the ferric-superoxo species was carried out by γ-ray irradiation of the sample at 77 K in 20% MeCN/2MeTHF (2MeTHF = 2-methyltetrahydrofuran). The EPR spectrum of the irradiated sample does not show a signal corresponding to a ferric heme, but rather a signal with $g_{//}$ = 2.10 is observed and the $g_{\perp}$ signal was hidden under the intense signals in the g = 2.0 region derived from radicals arising from solvent radiolysis (Fig. 1A).[22, 23] The $g_{//}$ = 2.10 signal is absent in the iron porphyrin-free sample composed of O_2 saturated solvent. When the irradiated sample is annealed at 173 K, the signal at g = 2.10 disappears and a new set of signals (g = [2.30, 2.17, 1.95]) ascribed to a low-spin ferric-hydroperoxo porphyrin is observed.[14] These observations clearly indicate that the species associated with the g = 2.10 signal is a ferrous-superoxo porphyrin species as reported previously (Scheme 1).[22,23]

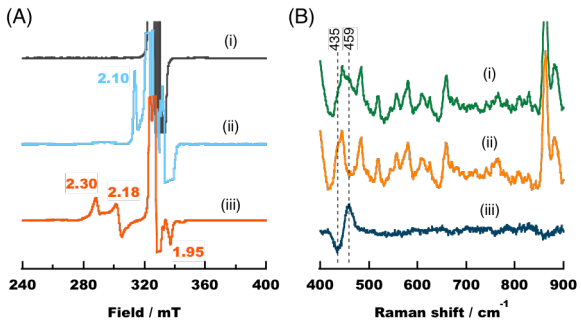

Fig. 1 (A) EPR spectra of the control sample (i), the γ-ray irradiated sample (ii) and the annealed sample (iii). (B) rR spectra of ferrous superoxo prepared by $^{16}O_2$ (i), $^{18}O_2$ (ii), and the difference ($^{16}O_2$ – $^{18}O_2$) (iii) obtained by 429.6 nm laser excitation at 77 K.

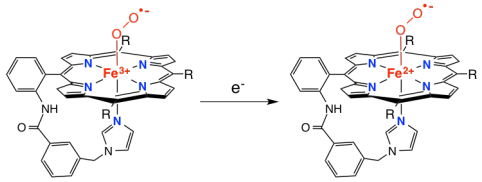

Scheme 1 Formation of ferrous-superoxo porphyrin upon one-electron reduction of ferric-superoxo porphyrin (R = mesityl group).

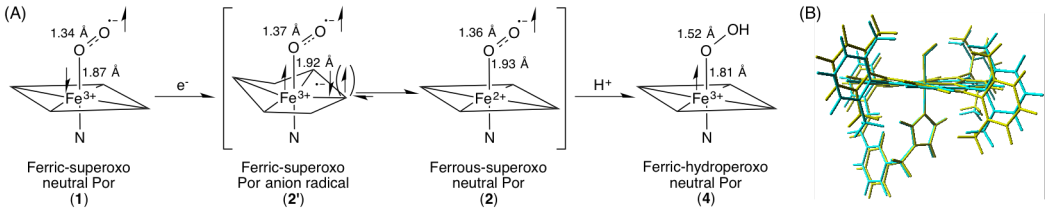

Fig. 2 (A) Schematic drawings of geometric and electronic structures of ferric-superoxo porphyrin (**1**), ferrous-superoxo porphyrin (**2**), ferric-superoxo porphyrin anion radical (**2'**), and ferric-hydroperoxo porphyrin (**4**). Squares and the distorted square indicate planar and ruffled iron porphyrin, respectively, and axial imidazole ligation is indicated by N. (B) Overlaid calculated structures of ferric-superoxo porphyrin anion radical (**2'**, S = 1/2)(yellow) and ferrous-superoxo porphyrin (**2**) (cyan).

Next, we carried out cryo-resonance Raman analyses on the ferrous-superoxy heme. Both $^{16}O_2$ and $^{18}O_2$ heme adducts were irradiated with γ-rays for rR analyses. The γ-ray irradiated sample shows an oxygen isotope sensitive band at 459 cm^{-1} (^{16}O)/435 cm^{-1} (-24 cm^{-1} for ^{18}O) (Fig. 1B). Thus the iron-oxygen stretching ($\nu_{Fe\text{-}O}$) frequency of the ferrous-superoxo is significantly lowered relative to that of the ferric-superoxo complex observed at 579 cm^{-1}. The low $\nu_{Fe\text{-}O}$ frequency is comparable to the $\nu_{Ni\text{-}O}$ frequency (437 cm^{-1}) observed in a Ni^{2+}-superoxo species.[24] The O-O stretching mode ($\nu_{O\text{-}O}$) was not observed, and this mode is known to be difficult to detect in the case of the ferric-superoxo complex unless a H-bond interaction is present for heme bound O_2.[25,26] In the high frequency region of the rR spectra, the ν_4 band of the heme shows a clear shift from 1367 cm^{-1} for the ferric-superoxo species to 1357 cm^{-1} for the irradiated sample, indicating that ferrous iron is involved (Fig. S2). Single electron reduction of the ferric-superoxy complex may yield a high-spin ferric side-on peroxo complex in the absence of an axial ligand.[27] However, heme iron is located in the plane of the porphyrin in the presence of an axial imidazole ligand stabilizing the end-on O_2 low-spin electronic configuration.[14,28,29] To the best of our knowledge, this is the first rR characterization of cryo-generated ferrous superoxo heme.

To rationalize the structure and reactivity of ferrous-superoxo species, DFT analyses were performed. The ferric-superoxo complex and its one-electron reduced species with a doublet spin state were geometry optimized using the B3LYP DFT functional. The choice of basis sets for the calculation includes the 6-311+G* for Fe, N_{por}, O_2 atoms, and the 6-31G* basis set was used for the rest of atoms (See the ESI).

Table 1 Spin densities of heme-O_2(H) intermediates[a]

	Fe	^{p}O	^{d}O	Cα	Cβ	Cm	N_{por}
1	-1.12	0.39	0.67	-0.03	-0.01	0.01	0.10
2'	1.11	0.35	0.58	-0.16	-0.29	-0.41	-0.18
2	0.18	0.41	0.55	-0.09	-0.04	-0.02	0.01
4	0.92	0.14	0.01	0.01	0.00	-0.01	-0.06

[a] The numbering scheme of intermediates is shown in Figure 2. ^{p}O and ^{d}O are proximal and distal O atoms with respect to Fe, respectively. Cα, Cβ, Cm are alpha, beta, and meso C atoms of porphyrin, respectively. N_{por} is four N atoms of porphyrin.

The Fe-O_2 and O-O bond distances of ferric-superoxy in the broken-symmetry singlet state were computed as 1.87 Å and 1.34 Å, respectively (Figs. 2 and S1), and nearly one spin density distributes in heme-bound-O_2 and the iron in an anti-parallel manner (Table 1). This is in good agreement with the computational results of Shaik and coworkers in terms of Fe-O_2 bond distance.[30] Upon one-electron reduction, ferrous-superoxo heme was expected to form. However, a ferric-superoxy porphyrin radical anion, in which the spins of Fe-O_2 (S = 1) and the porphyrin radical (S = 1/2) are coupled in an anti-parallel manner, was also optimized, lying 15.6 kcal/mol above the potential energy surface of the ferrous-superoxo species (Table S1).[31] Hessian analysis of the newly calculated electronic tautomer showed no imaginary eigenvalue indicative of a local minimum structure.[32] The formation of the radical anion is accompanied by distortion (ruffling) of the porphyrin plane (Figs. 2 and S1), implying that porphyrin deformation[33,34] is an important structural mechanism in the reactivity of O_2-activating heme catalysts.

The Fe-O_2 and O-O bond distances of the ferrous-superoxy species were calculated as 1.93 and 1.37 Å, respectively, while those of ferric-superoxy porphyrin radical anion were calculated as 1.92 and 1.36 Å, respectively. Thus, DFT calculations predict elongation of the Fe-O_2 bond in both cases compared to ferric-superoxy. This must be related to the observed 120 cm^{-1} downshift in Fe-O_2 stretching frequency. Vibrational frequency analysis of ferrous superoxo heme predicts that the Fe-O_2 stretching frequency is 500 cm^{-1}, showing fairly good agreement with the experimental result if a scaling factor of 0.96 is taken into consideration. An expanded porphyrin core calculated for the ferrous-superoxo compared to ferric-superoxo species is also consistent with the observation of the downshifted ν_2 band in the rR spectra (Fig. S1 and S3).

Protonation of the ferrous-superoxy species causes an increase of Fe-O_2 bond covalency with the bond distance of 1.81 Å with concomitant increase of the O-O bond distance to 1.52 Å, and nearly one spin is located on the iron, indicating formation of ferric hydroperoxy complex.

To elucidate the reaction mechanism of the ferrous-superoxy species, thermochemical analyses were performed as shown in Fig. 3. The reduction potential of the ferric-superoxo complex (**1**) to yield ferrous-superoxo (**2**) was calculated as -1.7 V (vs. SHE) in THF as one aprotic solvent. Complex **2** has high proton affinity with a pK_a of 39. In fact the cryo-generated ferrous-superoxy heme when annealed at -80 °C is protonated to yield a ferric-hydroperoxy complex even in the absence of any external proton source, indicating that it can abstract a proton from an adventitious water molecule in the solvent or from a cation radical species of 2MeTHF produced by γ-ray irradiation. The pK_a of the electronic tautomer of the ferric-superoxo porphyrin anion radical was calculated as 48, indicating high reactivity with respect to proton abstraction.

Reduction of the protonated oxy complex (**3**), the electronic structure of which can be described as a ferric porphyrin radical cation, involves a significantly higher positive potential of 0.6 V. In ORR, the PCET reaction would occur depending on the local proton concentration, and the reduction should occur at a potential between the value of the proton-assisted and the non-assisted mechanism. Thus, the incorporation of a proton donor into the active site is crucial to reduce the large thermodynamic barrier of the single

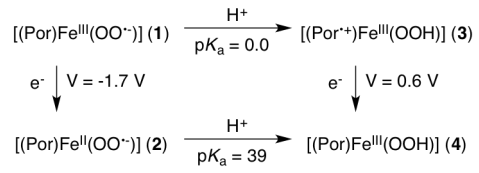

Fig. 3 DFT-calculated thermodynamic diagram of one-electron reduction and protonation of ferric-superoxo heme based on the Born-Haber cycle method in conjunction with a solvation model in THF (ε = 7.6). Complexes **1**, **2**, **3**, and **4** correspond to ferric-superoxy, ferrous-superoxy, protonated ferric-superoxy, and ferric-hydroperoxy complexes, respectively. The absolute potential of SHE used was 4.43 eV, and the hydration of proton ($\Delta G_{sol}(H^+)$) was assumed to be -266 kcal/mol (see the ESI).

electron reduction of the ferric-superoxy species. Design of a porphyrin-based oxygen reduction catalyst is a topic of current interest in energy conversion chemistry.[35-39]

In summary, the Fe-O_2 stretching frequency of the ferrous-superoxy species generated by cryo-reduction in an aprotic environment was characterized, and its formation and reactivity was rationalized by DFT calculations. The computational prediction of the structure and reactivity of the ferric-superoxy porphyrin neutral radical is intriguing considering porphyrin deformation is a common occurrence in protein matrices.[40]

This work was financially supported by Scientific Research (C) (no. 24550080) and Scientific Research on Innovative Area (no. 25109535) to TO from JSPS, by the Elemental Science and Technology Project to YN from the MEXT of Japan and by NSF of China (no 21271072), the Program for Professor of Special Appointment (Eastern Scholar) at Shanghai Institutions of Higher Learning, and the Shanghai Pujiang Program (no. 13J1401900) to JGL. Co-60 γ-ray irradiation was performed with assistance provided by Prof. Tomio Okai of the Department of Applied Quantum Physics and Nuclear Engineering, Kyushu University. DFT calculations were performed at the Research Center for Computational Science, Okazaki, Japan.

Notes and references

[a] *Picobiology Institute, Graduate School of Life Science, University of Hyogo, Hyogo 679-5148, Japan. Email: takehiro@sci.u-hyogo.ac.jp*
[b] *Institute for Materials Chemistry and Engineering, Kyushu University, Fukuoka 812-8581, Japan.*
[c] *Department of Chemistry, East China University of Science and Technology, 20237 Shanghai, China. Email: liujingang@ecust.edu.cn*
[d] *Institute of Science and Technology Research, Chubu University, Kasugai, Aichi 487-8501, Japan. Email: naruta@isc.chubu.ac.jp*
Electronic Supplementary Information (ESI) available: [Experimental and computational details]. See DOI: 10.1039/c000000x/

1 D. L. Wertz, J. S. Valentine, *Struct. Bonding (Berlin)*, 2000, **97**, 37–60, and references therein.
2 E. E. Chufan, S. C. Puiu and K. D. Karlin, *Acc. Chem. Res.*, 2007, **40**, 563-572.
3 W. Nam, *Acc. Chem. Res.*, 2007, **40**, 522–531.
4 L. Que Jr. and W. B. Tolman, *Nature*, 2008, **455**, 333–340.
5 J. T. Groves, *Proc. Natl. Acad. Sci. USA*, 2003, **100**, 3569–3574.
6 J. P. Collman, R. Boulatov, C. J. Sunderland and L. Fu, *Chem. Rev.*, 2004, **104**, 561–588.
7 T. Ohta., J. -G. Liu and Y. Naruta, *Coord. Chem. Rev.*, 2013, **257**, 407-413.
8 F. A. Armstrong and J. Hirst, *Proc. Natl. Acad. Sci. USA*, 2011, **108**, 14049-14054.
9 M. Sono, M. P. Roach, E. D. Coulter and J. H. Dawson, *Chem. Rev.*, 1996, **96**, 2841–2888.
10 I. G. Denisov, T. M. Makris, S. G. Sligar and I. Schlichting, *Chem. Rev.*, 2005, **105**, 2253–2277.
11 Y. Watanabe, H. Nakajima and T. Ueno, *Acc. Chem. Res.*, 2007, **4** 554–562.
12 T. Matsui, M. Iwasaki, R. Sugiyama, M. Unno and M. Ikeda-S *Inorg. Chem.*, 2010, **49**, 3602–3609.
13 K. Duerr, J. Olah, R. Davydov, M. Kleimann, J. Li, N. Lang, Puchta, E. Hübner, T. Drewello, J.N. Harvey, N. Jux and I. Ivanovi Burmazovic, *Dalton Trans.*, 2010, **39**, 2049–2056.
14 J. -G. Liu, T. Ohta, S. Yamaguchi, T. Ogura, S. Sakamoto, Y. Maeda and Y. Naruta, *Angew. Chem. Int. Ed.*, 2009, **48**, 9262–9267.
15 K.D. Karlin, *Nature*, 2010, **463**, 168–169.
16 S. P. de Visser, J.S. Valentine and W. Nam, *Angew. Chem. Int. Ed* 2010, **49**, 2099–2101.
17 K. Tajima, S. Oka, T. Edo, S. Miyake, H. Mano, K. Mukai, H. Saku and K. Ishizu, *J. Chem. Soc., Chem. Commun.*, 1995, 1507–1508.
18 T. Kamachi, Y. Shiota, T. Ohta and K. Yoshizawa, *Bull. Chem. So Jpn.*, 2003, **76**, 721-732.
19 T. Kitagawa and Y. Mizutani, *Coord. Chem. Rev.*, 1994, **135/136** 685–735.
20 J.-G. Liu, Y. Shimizu, T. Ohta and Y. Naruta, *J. Am. Chem. Soc.*, 2010, **132**, 3672–3673.
21 H. Kitagishi, M. Tamaki, T. Ueda, S. Hirota, T. Ohta, Y. Naruta and K. Kano, *J. Am. Chem. Soc.*, 2010, **132**, 16730–16732.
22 R. Davydov, J. D. Satterlee, H. Fujii, A. Sauer-Masarwa, D. H. Busch and B. M. Hoffman, *J. Am. Chem. Soc.*, 2003, **125**, 16340-16346.
23 N. Bartlett and M. C. Symons, *Biochim. Biophys. Acta*, 1983, **744** 110-114.
24 M. T. Kieber-Emmons, J. Annaraj, M. S. Seo, K. M. Van Heuvelen, Tosha, T. Kitagawa, T. C. Brunold, W. Nam and C. G. Riordan, *J. Am. Chem. Soc.*, 2006, **128**, 14230-14231.
25 T. K. Das, M. Couture, Y. Ouellet, M. Guertin and D. L. Rousseau, *Proc. Natl. Acad. Sci. USA*, 2001, **98**, 479-484.
26 T. Ohta, H. Yoshimura, S. Yoshioka, S. Aono and T. Kitagawa, *J. Am Chem. Soc.*, 2004, **126**, 15000-15001.
27 C. H. Welborn, D. Dolphin and B. R. James, *J. Am. Chem. Soc.*, 198 **103**, 2869-2870.
28 T. Ohta, J.-G. Liu, M. Saito, Y. Kobayashi, Y. Yoda, M. Seto and Naruta, *J. Phys. Chem. B*, 2012, **116**, 13831-13838.
29 I. Garcia-Bosch, S. M. Adam, A. W. Schaefer, S. K. Sharma, R. Peterson, E. I. Solomon and K. D. Karlin, *J. Am. Chem. Soc.*, 201 **137**, 1032-1035.
30 S. Shaik, D. Kumar, S. P. de Visser, A. Altun, W. Thiel, *Chem. Re* 2005, **105**, 2279-2328.
31 The quartet spin-state, in which the spin of Fe-O_2 (S = 1) is coupled with the porphyrin radical (S = 1/2) in a parallel manner, calculated to be more stable than the doublet spin-state by 0.8 kcal/ (Table S2).
32 A BP86 functional calculation was also performed to examine DFT functional dependency. The broken symmetry-like state obtained b the B3LYP calculation was also calculated by the BP86 functional the quartet spin-state, while the calculation in the doublet spin-st resulted in formation of a ferrous-superoxy species with a plan porphyrin. See supporting materials for further discussion.
33 M. Nakamura, T. Ikeue, Y. Ohgo, M. Takahashi and M. Takeda, *Che Comm.*, 2002, 1198-1199.
34 R.-J. Cheng, C.-W. Chao, Y.-P. Han, Y.-C. Chen and C.-H. Tin *Chem. Comm.*, 2009, 2180-2182.
35 P. J. Wei, G. Q. Yu, Y. Naruta and J.-G. Liu, *Angew. Chem. Int. Ed* 2014, **53**, 6659-6663.
36 K. Sengupta, S. Chatterjee, S. Samanta and A. Dey, *Proc. Natl. Acad. Sci. USA,* 2013, **110**, 8431-8436.
37 S. Y. Reece, J. M. Hodgkiss, J. Stubbe and D. G. Nocera, *Phil. T ns. R. Soc. B*, 2006, **261**, 1351-1364.
38 C. T. Carver, B. D. Matson and J. M. Mayer, *J. Am. Chem. Soc.*, 201 **134**, 5444-5447.
39 A. Schechter, M. Stanevsky, A. Mahammed and Z. Gross, *Inor Chem.*, 2012, **51**, 22-24.
40 J. A. Shelnutt, X.-Z. Song, J.-G. Ma, S.-L. Jia, W. Jentzen and C. J Medforth, *Chem. Soc. Rev.*, 1998, **27,** 31-41.